Atmospheric Environment 67 (2013) 1–12

Contents lists available at SciVerse ScienceDirect

Atmospheric Environment

journal homepage: www.elsevier.com/locate/atmosenv

Tracking of atmospheric release of pollution using unmanned aerial vehicles

Václav Šmídl*, Radek Hofman

Institute of Information Theory and Automation, Prague, Czech Republic

HIGHLIGHTS

- An algorithm for navigation of UAVs tracking atmospheric release is pro-posed.
- Dynamics of the release is unknown and estimated on-line on a fine time scale.
- Time varying biases of the numerical weather forecast are estimated.
- Assimilation methodology is based on the sequential Monte Carlo.
- Twin experiments performed on a release of radiation with realistic setting.

ARTICLE INFO

Article history:
Received 30 July 2012
Received in revised form
28 October 2012
Accepted 30 October 2012

Keywords:
Data assimilation
Atmospheric dispersion model
Sequential Monte Carlo
Sensor positioning
Mutual information

ABSTRACT

Tracking of an atmospheric release of pollution is usually based on measurements provided by stationary networks, occasionally complemented with deployment of mobile sensors. In this paper, we extend the existing concept to the case where the sensors are carried onboard of unmanned aerial vehicles (UAVs). The decision theoretic framework is used to design an unsupervised algorithm that navigates the UAVs to minimize the selected loss function. A particle filter with a problem-tailored proposal function was used as the underlying data assimilation procedure.

A range of simulated twin experiments was performed on the problem of tracking an accidental release of radiation from a nuclear power plant in realistic settings. The main uncertainty was in the released activity and in parametric bias of the numerical weather forecast. It was shown that the UAVs can complement the existing stationary network to improve the accuracy of data assimilation. Moreover, two autonomously navigated UAVs alone were shown to provide assimilation results comparable to those obtained using the stationary network with more than thirty sensors.

1. Introduction

Accidental release of a pollutant into the atmosphere is a rare event, however with severe consequences for potentially many people living in proximity of its source. Correct application of the protective measures requires the best possible knowledge about the source and the trajectory of the plume in the atmosphere. Since dispersion of the pollutant in the atmosphere is highly stochastic, every measurement is of a great value. This fact motivated the creation of stable monitoring networks, e.g. around nuclear power plants, and stable and mobile stations for general air quality monitoring that are routinely in operation. The use of airborne measuring stations is less frequent, they are typically assumed to be used only in cases of severe accidents. Since it is too risky to send human-operated aircrafts into the polluted area, these are assumed to be used in the post-accident analysis. With increasing availability of commercial unmanned aerial vehicles (UAVs) arises the question of their use in tracking of accidental atmospheric releases.

In principle, the UAVs have several important advantages. First, they can fly in three dimensional space without spatial restrictions, which contrasts with limits of road vehicles. Second, they can be relatively small and thus they can be deployed in a very short time. Third, as unmanned vehicles they can fly to dangerous zones. Fourth, their movement in the atmosphere is relative to the wind which provides (in combination with GPS) an additional source of information about the wind field.

In this paper, we study the advantages of using UAVs in tracking of an atmospheric release. This task has been considered before using expert system with manually selected rules (Kuroki et al., 2010). Here, we are concerned with fully automatic on-line navigation of the UAVs. We study two potential roles of UAVs: operation in a standalone mode, and operation as a complementary measurements to the existing monitoring networks. Operation in the complementary mode is possible in high profile applications such as radiation accidents, while the standalone mode may be

* Corresponding author. Tel.: +420 26605 2420; fax: +420 26605 2068.
E-mail address: smidl@utia.cas.cz (V. Šmídl).

1352-2310/$ – see front matter © 2012 Elsevier Ltd. All rights reserved.
http://dx.doi.org/10.1016/j.atmosenv.2012.10.054

interesting for less safety critical applications, such as chemical accidents.

From the methodological point of view, UAVs are mobile sensors that can be relocated at every sampling time. Their navigation is thus an extension of the task of a monitoring network design which has been studied for decades, from early works (Caselton and Husain, 1980) to recent ones (Abida and Bocquet, 2009; Heuvelink et al., 2010). The standard formalism for sensor positioning is the decision theory under uncertainty (Berger, 1985) that poses the task as a minimization problem with respect to the expected future loss function. Previously proposed approaches differ in three aspects: (i) representation of uncertainty, (ii) loss function, and (iii) optimization methods and constraints. The need for uncertainty representation limits the possible selection of the assimilation methodology. For example, traditional methods like point based estimates such as the variational (Jeong et al., 2005; Kovalets et al., 2009) or genetic approach (Haupt et al., 2009; Cervone et al., 2010) are not a natural choice. We need to choose from the methods that model uncertainty using a Gaussian density (Zidek et al., 2000; Abida and Bocquet, 2009), or an empirical density obtained by Monte Carlo trials (Heuvelink et al., 2010; Melles et al., 2011). The choice of the loss functions ranged from entropy (Zidek et al., 2000) to the number of misclassified people (Heuvelink et al., 2010). Since most authors aimed for the global optimum, the most popular choice of the optimization method was simulated annealing, e.g. (Abida et al., 2008; Melles et al., 2011).

A distinct feature of the UAVs as mobile sensors is the need to compute their new locations in real time. This puts practical constraints on the processing time of all elements of the method. As a first step, we relax the requirement of global optimality and seek only a suboptimal solution. We choose to represent the uncertainty via the weighted empirical density, which is provided by the particle filter (Pecha et al., 2009; Hiemstra et al., 2011). We combine both popular loss functions, i.e. the mutual information and the misclassification loss, into a single loss function for improved robustness and flexibility. Computational details of this approach are based on works from the field of UAV navigation (Skoglar, 2009; Hoffmann and Tomlin, 2010; Šmídl and Hofman, 2012b) and recent techniques for efficient Monte Carlo sampling (Šmídl and Hofman, 2012a).

The algorithms were tested in simulated twin experiments. Specifically, we simulate a release of a radioactive pollutant from a nuclear power plant, where the radiation monitoring network (RMN), also known as radionuclide monitoring network, is already in place. In this scenario, we investigate the added value of the UAVs as a complementary means of radiation situation assessment. For comparison, we also investigate the same release without the data from the RMN to investigate the value of UAVs for tracking of releases from less protected sources.

2. Theoretical background

Navigation of the UAVs will be formalized as the task of positioning J sensors, where J is the number of available UAVs. At each time step t, we seek new directions of flight of all UAVs, $\boldsymbol{v}_{1,t+1},\ldots,\boldsymbol{v}_{J,t+1}$, and their speeds $s_{1,t+1},\ldots,s_{J,t+1}$. These form the action variable $\boldsymbol{a}_{t+1} = [\boldsymbol{v}_{1,t+1},\ldots,\boldsymbol{v}_{J,t+1},s_{1,t+1},\ldots,s_{J,t+1}]$. Following the standard decision theory (Berger, 1985), we optimize the expected loss

$$\boldsymbol{a}^*_{t+1} = \arg\min_{\boldsymbol{a}_{t+1}\in\mathcal{A}_{t+1}} E(\mathcal{L}(\boldsymbol{x}_{t:t+h},\boldsymbol{a}_{t+1:t+h})|y_{1:t}), \quad (1)$$

where $\boldsymbol{x}_{t:t+h} = [\boldsymbol{x}_t,\ldots,\boldsymbol{x}_{t+h}]$ is the uncertain future trajectory of the state variable, $\boldsymbol{x}_t$; $\mathcal{L}(\boldsymbol{x},\boldsymbol{a})$ is the loss function mapping the space of all actions and states to the real axis; $\boldsymbol{y}_{1:t} = [\boldsymbol{y}_1,\ldots\boldsymbol{y}_t]$ are the measured data; $E(\cdot)$ is the operator of expected value with respect to a probability density function $p(\cdot)$ of the random variable in argument of the expectation; $\mathcal{A}_{t+1}$ is a set of all possible actions at time $t+1$.

Framework (1) is very common in the field of network design and targeting of observations. Different methods arise for different choices of the unknown state variable $\boldsymbol{x}_t$, representation of uncertainty in the form of probability density $p(\cdot)$, and the loss function $\mathcal{L}(\cdot)$. In this paper, we will focus on the following variants. Distribution of the pollutant in the atmosphere is described by a parametric atmospheric dispersion model (e.g. the puff model) with unknown parameters. The weather model is based on local correction of the numerical weather forecast model. The state variable $\boldsymbol{x}_t$ is then quite low dimensional, composed of the parameters of the dispersion model and the weather corrections. The uncertainty in all parameters is represented by empirical probability densities (Johannesson et al., 2004). The loss function is based on combination of the misclassification loss (Heuvelink et al., 2010) and the mutual information (Hoffmann and Tomlin, 2010). These elements are now described in detail.

2.1. Atmospheric dispersion model

When the pollutant is released into the atmosphere, it forms a plume which is subject to dispersion. Various parametric models of the pollutant dispersion have been proposed. Here, we focus on approximation of the continuous plume by a collection of puffs (Thykier-Nielsen et al., 1999) for its simplicity. However, no subsequent derivation is based on this assumption and it can be replaced by any other parametric dispersion model. The puff model is formed by a sequence of puffs labeled $k = 1,\ldots,K$, each puff is assumed to approximate a short period of the release of the pollutant at discrete time t. Concentration of the pollutant in a single puff at time τ is given by:

$$C_k(\boldsymbol{s},\tau) = \frac{Q_k}{(2\pi)^{3/2}\sigma_1\sigma_2\sigma_3}\exp\left[-\frac{(s_1-l_{1,k,\tau})^2}{2\sigma_1^2} - \frac{(s_2-l_{2,k,\tau})^2}{2\sigma_2^2} - \frac{(s_3-l_{3,k,\tau})^2}{2\sigma_3^2}\right] \quad (2)$$

where $\boldsymbol{s} = [s_1,s_2,s_3]$ is a vector of spatial coordinates, $\boldsymbol{l}_{k,\tau} = [l_{1,k,\tau},l_{2,k,\tau},l_{3,k,\tau}]$ is the vector of location of the kth puff center, $\boldsymbol{\sigma} = [\sigma_1,\sigma_2,\sigma_3]$ are dispersion coefficients, and Q_k is the released activity in the kth puff. Released activity Q_k is assumed to be unknown, with very flat prior density, e.g. of gamma type

$$\mathcal{G}(\alpha_Q,\beta_Q) \propto Q_t^{\alpha_Q-1}\exp(-Q_t\beta_Q), \quad (3)$$

with parameters α_Q,β_Q. Symbol $\propto$ denotes equality up to normalizing constant. The prior parameters can be designed to match apriori chosen moments, e.g. the mean value, α_Q/β_Q, and the variance, α_Q/β_Q^2.

Illustration of the pollution model is displayed in Fig. 1. Spatial distribution of the pollutant is then fully determined by state variables:

$$\boldsymbol{x}_{pm,t} = \left[\boldsymbol{l}_{1,t}\ldots\boldsymbol{l}_{K,t},Q_{1,t},\ldots Q_{K,t},\boldsymbol{\sigma}_{1,t},\ldots\boldsymbol{\sigma}_{K,t}\right]. \quad (4)$$

2.2. Wind field model

We assume that the pollutant is released from a source at known location, $[s_{1,pp},s_{2,pp}]$ and known altitude $s_{3,pp}$, in vector notation, $\boldsymbol{s}_{pp} = [s_{1,pp},s_{2,pp},s_{3,pp}]$. From this point it is advected by the wind field. While it is possible to obtain numerical weather forecast from various sources, its accuracy is usually not sufficient at the

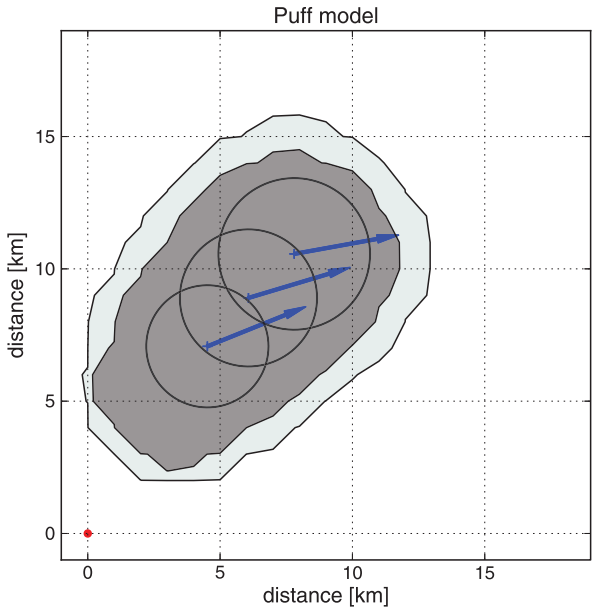

Fig. 1. Illustration of composition of the puff model for release of 6 puffs. Contours denote levels of the radiation dose and every second puff is displayed as a circle with diameter 3σ. Current wind field is illustrated by arrows in the center of each puff.

location of the potential release. An illustration of this fact is displayed in Fig. 2 by comparison of the wind direction obtained from the ALADIN numerical weather forecast and from the meteostation at the nuclear power plant Temelin.

Therefore, we locally calibrate the numerical weather model as follows:

$$v_t(\boldsymbol{s}) = \tilde{v}_t(\boldsymbol{s})\theta_{v,t}, \tag{5}$$

$$\phi_t(\boldsymbol{s}) = \tilde{\phi}_t(\boldsymbol{s}) + \theta_{\phi,t} + \theta_{c,t}\|\boldsymbol{s}-\boldsymbol{s}_0\|, \tag{6}$$

where $\tilde{v}_t(\boldsymbol{s})$, $\tilde{\phi}_t(\boldsymbol{s})$ are the wind speed and wind direction predicted by the numerical model at location $\boldsymbol{s}$, respectively. $\boldsymbol{s}_0$ is the location of the meteo-station and $\|\cdot\|$ denotes Euclidean distance. Constants $\boldsymbol{\theta}_t = [\theta_{v,t},\theta_{\phi,t},\theta_{c,t}]$ are unknown biases of the numerical weather forecast model at time t. Correction of the wind field forecast is then achieved by estimation of $\theta_{v,t},\theta_{\phi,t}$ and $\theta_{c,t}$ using random walk model on their time evolution, such as

$$\text{mean}(\theta_{v,t}) = \theta_{v,t-1}, \quad \text{std}(\theta_{v,t}) = \gamma_v\theta_{v,t-1} + \gamma_{v0}, \tag{7}$$

$$\text{mean}(\theta_{\phi,t}) = \theta_{\phi,t-1}, \quad \text{std}(\theta_{\phi,t}) = \gamma_\phi, \tag{8}$$

$$\text{mean}(\theta_{c,t}) = \theta_{c,t-1}, \quad \text{std}(\theta_{c,t}) = \gamma_c, \tag{9}$$

where parameters $\gamma_v,\gamma_{v0},\gamma_\phi,\gamma_c$ govern the variability of the biases in time. Given informative measurements, even these parameters can be estimated from the data. Constants $\theta_{v,t}$ and $\theta_{\phi,t}$ are commonly used corrections for the wind speed and direction (Hiemstra et al., 2011). The third coefficient, $\theta_{c,t}$, models increasing deviation of the forecast with distance from the source.

Given wind field (5)–(6), center of the ith puff moves deterministically according to

$$\begin{aligned} l_{1,i,t+1} &= l_{1,i,t} + v_t(\boldsymbol{l}_{i,t})\sin(\phi_t(\boldsymbol{l}_{i,t})), \\ l_{2,i,t+1} &= l_{2,i,t} + v_t(\boldsymbol{l}_{i,t})\cos(\phi_t(\boldsymbol{l}_{i,t})). \end{aligned} \tag{10}$$

Dispersion coefficients $\boldsymbol{\sigma}$ are deterministic functions of the total traveled distance from the source and the Pasquill's stability category. The complete uncertainty about the future trajectory of the pollutant is then $\boldsymbol{x}_t = [\boldsymbol{x}_{pm,t},\boldsymbol{\theta}_t]$.

2.3. Loss function

We briefly review typical loss functions used in the literature. In the whole section we assume that the decision horizon h in (1) is only one step ahead, $h = 1$. Generalization to longer horizons is straightforward, but yields computationally more demanding algorithms.

2.3.1. Entropy and mutual information

The purpose of the positioning a new mobile measuring station is to reduce uncertainty in the estimated parameters. This idea can be formalized using the joint entropy of the state and the observations (Caselton and Husain, 1980; Zidek et al., 2000).

$$H(\boldsymbol{x}_{t+1},\boldsymbol{y}_{t+1}) = -\int p(\boldsymbol{x}_{t+1},\boldsymbol{y}_{t+1}|\boldsymbol{y}_{1:t},\boldsymbol{a}_t)\log p(\boldsymbol{x}_{t+1},\boldsymbol{y}_{t+1}|\boldsymbol{y}_{1:t},\boldsymbol{a}_t)\mathrm{d}\boldsymbol{x}_{t+1}\mathrm{d}\boldsymbol{y}_{t+1}. \tag{11}$$

Loss function in the form of (11) is suitable only for a limited class of observation models. In general, the mutual information loss

$$I(\boldsymbol{x}_{t+1};\boldsymbol{y}_{t+1}) = H(\boldsymbol{y}_{t+1}) + H(\boldsymbol{x}_{t+1}) - H(\boldsymbol{x}_{t+1},\boldsymbol{y}_{t+1}). \tag{12}$$

is a better choice (Hoffmann and Tomlin, 2010). Since $H(\boldsymbol{x}_{t+1})$ can not be influenced by actions $\boldsymbol{a}_t$, we need to evaluate (11) and

$$H(\boldsymbol{y}_{t+1}) = -\int p(\boldsymbol{y}_{t+1}|\boldsymbol{y}_{1:t},\boldsymbol{a}_t)\log p(\boldsymbol{y}_{t+1}|\boldsymbol{y}_{1:t},\boldsymbol{a}_t)\mathrm{d}\boldsymbol{y}_{t+1}. \tag{13}$$

2.3.2. Misclassification of decision

An alternative loss function for the purpose of population protection is defined with respect to the final decision on the countermeasures. Typically, the limits for the introduction of countermeasures are given in the form of threshold on a quantity of interest $d_t(\boldsymbol{s})$ at location $\boldsymbol{s}$. The countermeasures are introduced if the expected value $E(d_t(\boldsymbol{s})) > \overline{d}$, where $\overline{d}$ it the prescribed threshold.

A suitable loss function is then to minimize the error of classification, potentially weighted by the number of affected people (Heuvelink et al., 2010):

$$L_{miss}(\boldsymbol{x}_{t+1},\boldsymbol{a}_t) = \alpha L_{fp} + \beta L_{fn}, \tag{14}$$

where L_{fp} is the number of people incorrectly classified for the countermeasure, L_{fn} is the number of people that are incorrectly classified to stay in the polluted area, and α,β are the costs associated with incorrect decisions. We split the area around the source

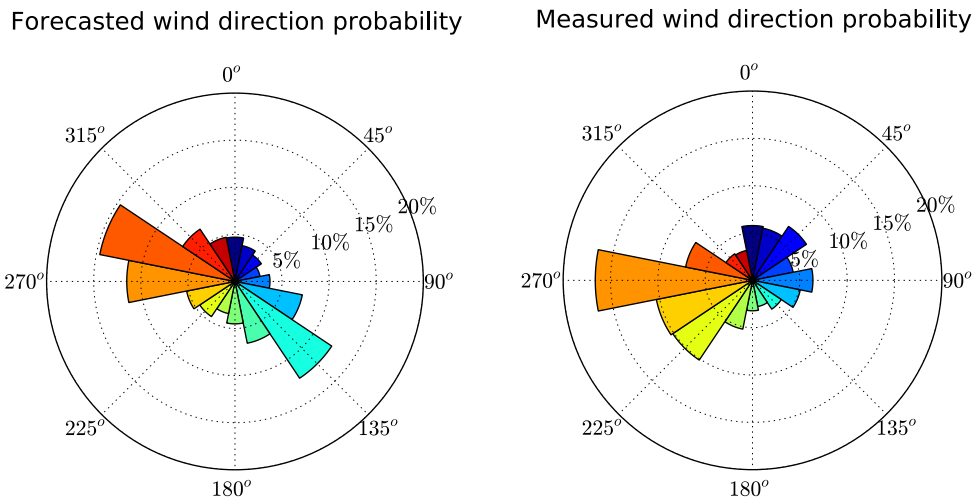

Fig. 2. Comparison of histograms of the wind direction at the location of the power plant Temelin for year 2008 from the ALADIN numerical model (left) and observed data (right).

of the release into M subareas, each representing a constant number of inhabitants, e.g. 100, each with a predefined location, $\boldsymbol{i}_m$, $m = 1\ldots M$. The total number of incorrectly classified inhabitants is then

$$L_{fp} = \sum_{m=1}^{M} E\left(\widehat{d}(\boldsymbol{i}_m) > \overline{d} \& d(\boldsymbol{i}_m) < \overline{d}\right), \tag{15}$$

$$L_{fn} = \sum_{m=1}^{M} E\left(\widehat{d}(\boldsymbol{i}_m) < \overline{d} \& d(\boldsymbol{i}_m) > \overline{d}\right), \tag{16}$$

where $\widehat{d}$ is defined as a point estimate of the quantity of interest. Symbols $>$ and $<$ are used in the sense of logical operators, i.e. its result is one if the condition is met and zero otherwise. Symbol & represents logical AND where the zeros and ones from the inequalities are treated as boolean values. The expectations in (15)–(16) are evaluated with respect to random variables $\boldsymbol{x}_{t+1}$ and $\boldsymbol{y}_{t+1}$.

2.3.3. Combined loss function

The main advantage of the misclassification loss function is its focus on the final decision that needs to be made, i.e. the countermeasures. However, it also suffers from higher granularity than the mutual information. In the extreme case, when the release becomes significantly lower than the threshold, the loss function is equal to zero for all possible UAV positions. To increase robustness of the decisions, we propose to combine the two loss functions into one

$$L(\boldsymbol{x}_{t+1}, \boldsymbol{a}_t) = \alpha L_{fp} + \beta L_{fn} + I(\boldsymbol{x}_{t+1}; \boldsymbol{y}_{t+1}) + L_a(\boldsymbol{a}_t), \tag{17}$$

where $L_a(\boldsymbol{a}_t)$ is a term reserved for the preference of the UAVs. This term will be specific to the used machine and its purpose is to supervise practical issues of the UAV, such as its fuel consumption and safe return to the base station.

Note that the coefficients α,β need to be tuned relatively to the mutual information.

3. Particle filter for data assimilation

We assume that all uncertainty is modeled by an empirical probability density function

$$p(\boldsymbol{x}_{1:t}|\boldsymbol{y}_{1:t}) \approx \sum_{n=1}^{N} w_t^{(n)} \delta(\boldsymbol{x}_{1:t} - \boldsymbol{x}_{1:t}^{(n)}), \tag{18}$$

where $\boldsymbol{x}_{1:t}^{(n)}$, $n = 1,\ldots,N$, is a sample of the state space trajectory. Assimilation of the measured data is then achieved via sampling-importance-resampling procedure, where the weights can be computed recursively,

$$w_t^{(n)} \propto w_{t-1}^{(n)} \frac{p(\boldsymbol{y}_t|\boldsymbol{x}_t)p(\boldsymbol{x}_t|\boldsymbol{x}_{t-1})}{q(\boldsymbol{x}_t|\boldsymbol{y}_t)}. \tag{19}$$

The proposal (importance) density $q(\boldsymbol{x}_t|\boldsymbol{y}_t)$ can be chosen arbitrarily, however its choice severely impacts computational requirements of the filter. Good resampling strategy is also necessary to prevent degeneracy of the particle filter (19) (Doucet et al., 2001).

3.1. Measurement models

3.1.1. Measurements of the wind field

We assume that the wind direction and velocity can be measured by stationary sensors as well as by the UAVs themselves (van den Kroonenberg et al., 2008). For simplicity, we assume that the measurements of the wind speed are Gamma distributed around the true value with standard deviation of the observation $\mathrm{std}(v_t) = \gamma_v v_t(\boldsymbol{s}_0)$, and the measurements of the wind direction are Gaussian[1] distributed around the true value with constant $\mathrm{std}(\phi_t) = \sigma_\phi$. These values are typically available from the manufacturers of the sensors. Accuracy of the measurements from the UAVs may be harder to calibrate, however, results in (van den Kroonenberg et al., 2008) indicate that accuracy of the measurements is comparable to that of the stationary sensors.

3.1.2. Measurements of the pollutant

Direct measurements of the pollutant concentrations are often assumed (Johannesson et al., 2004; Abida and Bocquet, 2009). In the radiation application, it may not be always possible and an additional transformation requiring spatial and temporal integration of the concentration is needed (Šmídl and Hofman, 2012a). However, in both situations, the error of measurement is assumed

[1] More exactly, it is distributed as a wrapped Gaussian density (Mardia and Jupp, 2000). However, the difference from the regular Gaussian density is negligible for the considered values of σ_ϕ.

to be relative to its value and the measured value from one puff is linear in the released activity. Therefore, we analyze measurements of the concentration, treatment of the gamma dose detector in the radiation case requires more computation but is completely analogous from the assimilation point of view.

Since the release is composed of many puffs, the true concentration at the jth sensor is the superposition of contributions from all puffs and natural background, c_{bg}:

$$c_{j,t} = \sum_{k=1}^{K} Q_k \rho_{k,j,t} + c_{bg}, \quad \rho_{k,j,t} = \int_{t-1}^{t} Q_k^{-1} C_k(\boldsymbol{s}_j, \tau) \mathrm{d}\tau. \tag{20}$$

The measured value of the concentration at the jth sensor, $y_{j,Q,t}$, is assumed to have inverse Gamma density with relative error, $\gamma_y \in \langle 0, 1 \rangle$,

$$p\left(y_{j,t} \middle| Q_{1:t}\right) = i\mathcal{G}(\alpha_y, \beta_y) \propto y_{j,t}^{-\alpha_y - 1} \exp\left(-\beta_y y_{j,t}^{-1}\right), \tag{21}$$

where $\alpha_y = \gamma_y^{-2} + 2$, $\beta_y = (\alpha_y - 1)c_{j,t}$. Note that the sensors can be either stationary or mounted on the UAVs. Since position of the UAVs is changing in time, the integration path over $\boldsymbol{s}_j$ in (20) needs to be adjusted. We assume linear interpolation of the UAVs' positions between $\boldsymbol{a}_t$ and $\boldsymbol{a}_{t+1}$.

3.2. Proposal density

In principle, it would be possible to use the popular bootstrap particle filter (Gordon et al., 1993) to obtain the assimilated results. However, it would be computationally inefficient. More computationally efficient proposal densities can be designed by approximation of the optimal proposal density (Doucet et al., 2001). In this paper, we use the conditionally independent proposal density suggested in (Šmídl and Hofman, 2012a). Many elements of the state variable evolve deterministically, e.g. the locations of the puff's centers $\boldsymbol{l}_t$ and the old values of the released dose Q_t. The only elements of $\boldsymbol{x}_t$ that need to be sampled are Q_t, θ_t. Within these elements, we impose the following conditional independence structure,

$$\begin{aligned} q(Q_t, \boldsymbol{\theta}_t | \boldsymbol{x}_{t-1}, \boldsymbol{y}_t) \equiv \\ q(Q_t | y_t, Q_{t-1}) q(\theta_{v,t} | \boldsymbol{y}_t, \theta_{v,t-1}) \\ \times q\left(\theta_{\phi,t}, \theta_{c,t} | \boldsymbol{y}_t, \boldsymbol{\theta}_{t-1}\right). \end{aligned} \tag{22}$$

the optimal proposal densities for $q(\theta_{v,t} | \boldsymbol{y}_t, \theta_{v,t-1})$, $q(\theta_{\phi,t}, \theta_{c,t} | \boldsymbol{y}_t, \boldsymbol{\theta}_{t-1})$ can be found analytically, see Appendix A.1. Proposal density for $q(Q_t | \boldsymbol{y}_t)$ is still intractable, but the Laplace approximation (Kass et al., 1990) was found to provide suitable approximation, see Appendix A.2.

3.3. Navigation of the UAVs

We assume that within the sampling period, the UAVs can fly at a maximum speed $s_{\max}$. Hence, we discretize the space of potential actions into R points on polar coordinates where the edge is reachable at the maximum speed of the UAV, see Fig. 3 for illustration. The total number of potential decisions in $\mathcal{A}_{t+1}$ for one-step-ahead optimization is then R^I.

Optimal decisions are obtained by evaluation of one-step-ahead optimization of the chosen loss function for all combinations of the potential decisions. Sampling time of the decisions is 10 min. The decision is then submitted as a setpoint to the UAVs that navigate to the given coordinates autonomously.

The loss function (17) contains integrals over the future values of the state and the observations that need to be evaluated numerically. From the range of potential approaches (Šmídl and Hofman, 2011), we selected the importance sampling approach. Specifically, we approximate expected values of the loss such as (13) by:

$$H(\boldsymbol{y}_{t+1}) \approx \sum_{\lambda=1}^{\Lambda} \log p\left(\boldsymbol{y}_{t+1}^{(\lambda)} | \boldsymbol{y}_{1:t}, \boldsymbol{a}_t\right), \tag{23}$$

where $\boldsymbol{y}_t^{(\lambda)}$, $\lambda = 1 \ldots \Lambda$, are samples from $p(\boldsymbol{y}_{t+1} | \boldsymbol{y}_{1:t}, \boldsymbol{a}_t)$. In all simulations, we used the same number of hypothetical measurements $\boldsymbol{y}_{t+1}^{(\lambda)}$ as the number of particles, i.e. $\Lambda = N$.

Evaluation of the misclassification loss is analogous,

$$L_{fp} \approx \sum_{m=1}^{M} \sum_{\lambda=1}^{\Lambda} \left(\widehat{d}^{(\lambda)}(\boldsymbol{i}_m) > \overline{d} \,\&\, d^{(\lambda)}(\boldsymbol{i}_m) < \overline{d} \right), \tag{24}$$

where

$$\widehat{d}^{(\lambda)}(\boldsymbol{i}_m) = \sum_{i=1}^{I} w_{i,t}^{(\lambda)} d\left(\boldsymbol{i}_m, \boldsymbol{x}_{t:t+h}^{(i)}\right), \; w_t^{(\lambda)} \propto \frac{p\left(\boldsymbol{y}_{t+1}^{(\lambda)} | \boldsymbol{x}_{t+1}^{(i)}\right)}{\sum_{i=1}^{I} p\left(\boldsymbol{y}_{t+1}^{(\lambda)} | \boldsymbol{x}_{t+1}^{(i)}\right)}.$$

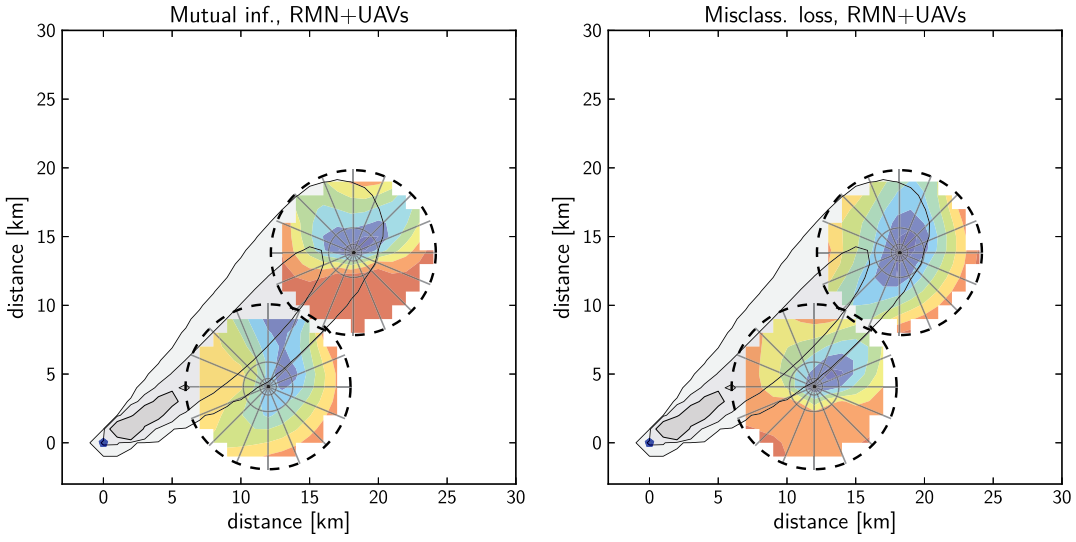

Fig. 3. Illustration of two loss functions evaluated at the same time for the same measurements in selected flight direction and flight speed for each UAV. Contour plots in the action radius of each UAV illustrate the loss function for its positioning given the best possible location of the other UAV.

Remark 1. We have chosen the total absorbed dose per person as our quantity of interest d. This is an integral quantity and needs to be evaluated on a long horizon, $\boldsymbol{x}_{t:t+h}$. However, we still consider uncertainty only in $\boldsymbol{x}_{t+1}$ and optimize only action variable $\boldsymbol{a}_t$, prediction of the future evolution of the cloud is deterministic for each particle, using fixed values of the correction coefficients $\boldsymbol{\theta}_{t+h} = \boldsymbol{\theta}_{t+1}$ and $Q_{t+h} = 0$, for $h > 2$.

4. Results and discussion

In this Section, we demonstrate added value of the UAVs for the tracking of atmospheric release in two scenarios from radiation protection. This application domain is chosen because nuclear power stations are equipped with stationary monitoring networks (RMN) which allows to study the use of UAVs as complementary measuring devices. For comparison, we also run the assimilation procedure without the data from the RMN.

4.1. Release parameters

A hypothetical one hour long release of radionuclide ^{41}Ar from a nuclear power station was simulated. This radionuclide was chosen as to reduce computational cost of the experiments for two reasons: (i) it is a noble gas which has no deposition and consequently no groundshine, hence we need to calculate only the gamma dose rate from cloudshine; (ii) it emits gamma radiation at energy level 1293.57 keV with branching ratio 99.1% and thus can be treated as a mono-energetic nuclide.

Other parameters of the release, such as the locations of the RMN sensors, the position of the meteostation, the locations of the inhabited areas and the typical weather conditions were calibrated for a hypothetical release from the Czech nuclear power plant Temelin.

The simulated release started at time $t = 1$ with release of one puff every 10 min with activity $Q_{1:6} = [1,5,4,3,2,1] \times 1e16Bq$ and $Q_t = 0$, for $t > 6$. The released activity was chosen high enough to reach a realistic level of the total absorbed dose needed for the misclassification loss function. Data assimilation is performed in time steps $t = 1,\ldots,21$, with sampling period of 10 min. This sampling period was chosen to match the sampling period of the RMN which provides measurements of time integrated dose rate in 10-min intervals. The same period was assumed for the anemometer. Values of the measurements were simulated as random draws from the measurement model (21) with mean values given by the twin model. The measurements are assumed to have standard deviation of 20% for the radiation dose, this estimate is based on conservative estimates of the accuracy of the gamma dose sensors (Thompson et al., 2000).

The forecast of the wind field was assumed to be homogeneous over the numerical computational grid for clarity of presentation, with values $\tilde{v}_t = 4$ m/s, $\tilde{\phi}_t = 80^\circ$ and Pasquill's class of stability D. This forecast is common in the locality of the power plant. A twin experiment was simulated with bias of the wind forecast according to the model (5)–(6) with parameters $\theta_{v,t} = 0.75$, $\theta_{\phi,t} = 20^\circ$, $\theta_{c,t} = -0.02$. Relatively high variability of the biases in time was assumed, specifically, $\gamma_v = 20\%$, $\gamma_\phi = 20^\circ$, $\gamma_c = 0.01$. Standard deviations of the measurements were estimated from real data measured at similar meteorological conditions, yielding 5% for the wind speed and 5° for the wind direction.

The presented scenario is rather simplistic and represents a favorable situation for the data assimilation. Its purpose is to present a proof of concept of the approach. More demanding scenarios can be also handled by the presented methodology, however, more careful modeling of the weather conditions, technical details of the release and computational issues need to be resolved. These issues are beyond the scope of this paper and left for further research.

4.2. Assimilation with RMN only

Contour plots of the total cloudshine dose after 3 h are displayed in Fig. 4 for the numerical forecast, the twin model and the result of particle filter assimilation using data from the RNM (denoted by blue dots), respectively. The results of assimilation were obtained using algorithm in Appendix A with 99 particles. This setup will be used for all subsequent assimilation procedures.

Note that the contour plot of the release assimilated using only the RMN covers larger area than that of the twin model. In effect, the estimate of the particle filter is a weighted superposition of N simulated plumes with different parameters. If the measured data can not distinguish which parameter values are relevant, all possible realizations must be considered. Since the RMN has a ring of sensors around the power plant, the released activity, $Q_{1:6}$, is estimated with high accuracy, Fig. 6 top left. Due to the meteostation at the power plant, the wind speed and direction biases, $\theta_{v,t}$

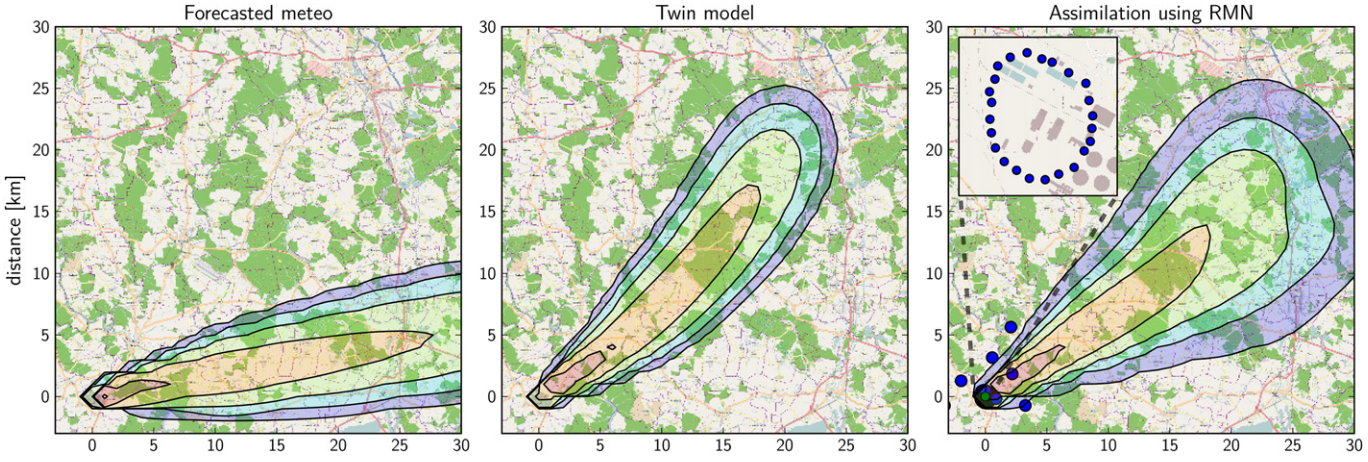

Fig. 4. Contour plots of the predicted total cloudshine dose in time $t = 18$. **Left**: Prediction based on the forecasted wind field. **Middle**: Twin model representing the reality by a biased wind field. **Right**: Result of assimilation using only measurements from the RMN. The exact locations of the sensors in the first ring of the RMN are displayed in the magnification in the top left corner.

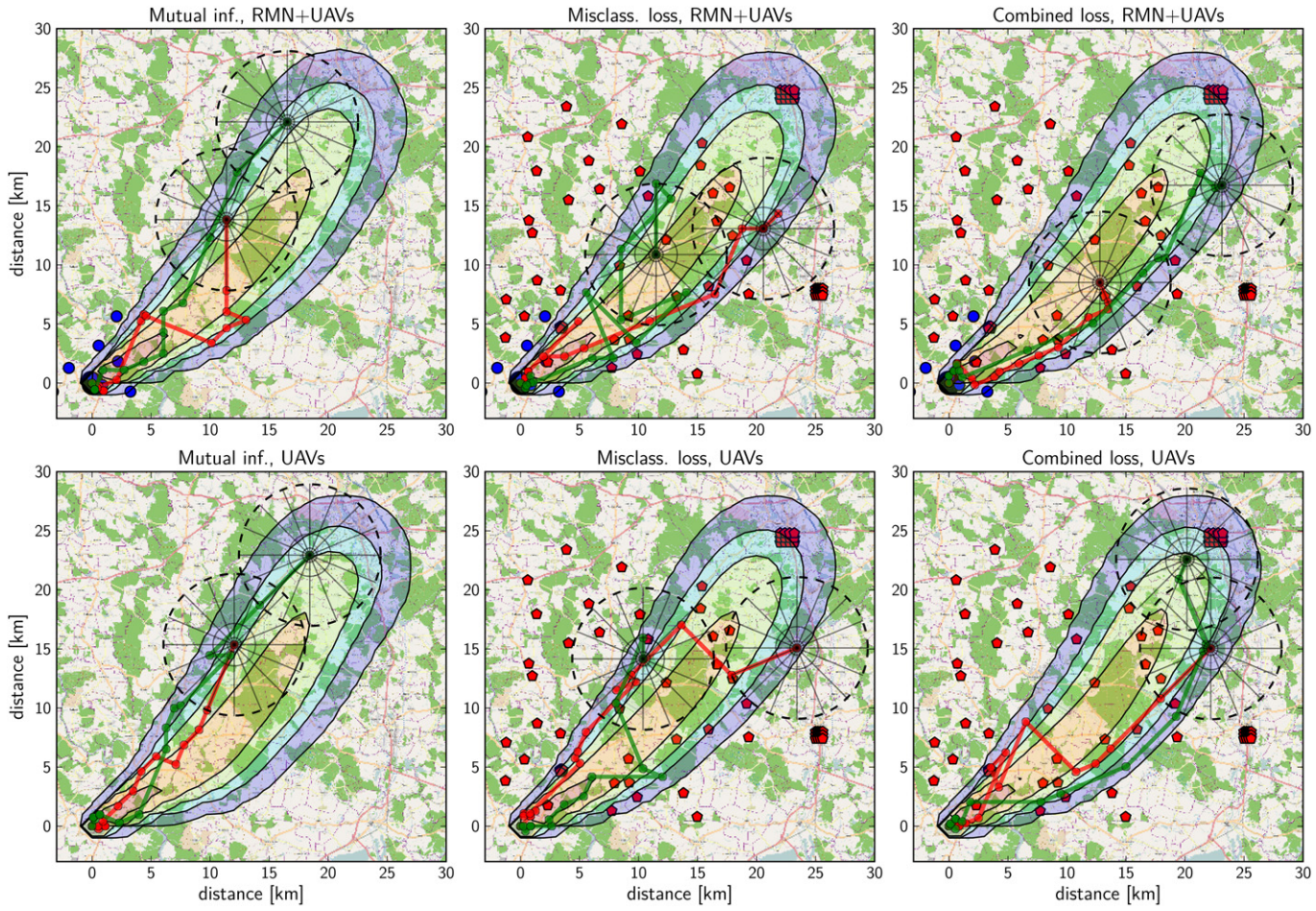

Fig. 5. Typical contour plots of the total cloudshine dose in time $t = 18$ (3 h after the release start) for different loss functions used to navigate the UAVs. The pentagons denote positions of the inhabited areas used in the misclassification loss. **Top row**: The data assimilation procedure is using data from the RMN and the UAVs. **Bottom row**: The data assimilation procedure is using only data from the UAVs. Locations of the UAVs at each time step are connected with thick lines.

and $\theta_{\phi,t}$, are also estimated with good accuracy. However, due to sparsity of the second and the third ring of the RMN and unavailability of the wind field measurements outside of the power plant, the most uncertain parameter is the straight line wind deviation, $\theta_{c,t}$. It is the uncertainty in $\theta_{c,t}$ that causes the increasing spread of the estimated plume with the distance from the source. This result highlights the attractive feature of the particle filtering that the uncertainty is not underestimated and the estimated contour plot includes the values of the twin model.

4.3. Data assimilation with the UAVs

Assimilation of the release was repeated with two autonomously navigated UAVs. In each time step, each the UAV considered 49 combinations of its flight direction and speed, displayed in the last point in UAV trajectory in Fig. 5. The global optimization then evaluated the loss function for 49^2 combinations and navigated each UAV according to the course with the lowest loss function. The results for three loss functions—(i) mutual information (12), (ii) misclassification loss (14), and (iii) the combined loss (17)—are displayed in Fig. 5. In the top row, the assimilation algorithm is using the data from the RMN and these data are also included in the evaluation of the loss functions. Note that with the UAVs, the expected values of the total cloudshine dose are almost identical for all considered loss functions. The trajectories of the UAVs are different for each loss. However, since the released activity is estimated well (Fig. 6), the most valuable measurement from the UAVs is the wind field measurement that allows estimation of the parameter $\theta_{c,t}$, which is provided under all considered loss functions. Specifically, the wind direction measurements allow efficient estimation of the bias parameter via optimal proposal (Appendix A.1). Estimation of the same parameter from the radiation dose measurements is less reliable and more computationally demanding.

In the complementary mode, the value of the UAVs is mainly in determination of the weather conditions, since the radiological quantities are determined well by the RMN. The drones typically move at the edge of the plume, which is consistent with findings of Abida and Bocquet (2009). The edge is found as a balance of two factors. First, the Gaussian shape of the pollutant dispersion in space and relative measurement error increase informativeness of the measurements with growing distance from the puff's center. Second, the constant term from the natural radiation background increases the relative error of measurements and thus decreases informativeness with distance form the center. The location of the optimal edge of the plume is thus determined by the measurement model and its parameters.

The same experiment was repeated without the measurements from the RMN and using only the measurements from the UAVs. The most significant change is in the accuracy of estimation of the released activity, see Fig. 6, bottom row. The mean value is still close to the simulated values, however, the variance is much larger. The

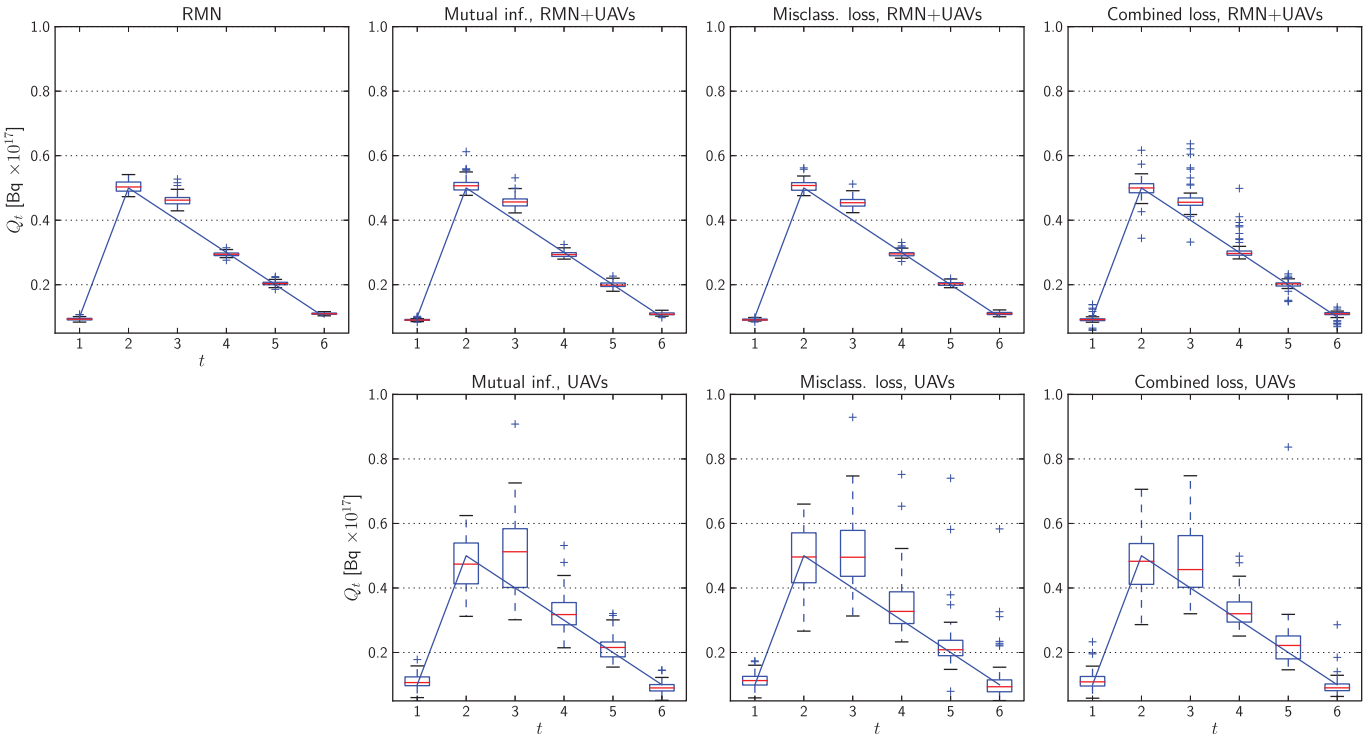

Fig. 6. Box plots of the expected value of the released activity, $Q_{1:6}$, from 50 random simulations. Solid lines represent the values of the twin simulation. **Top row**: Using measurements from the RMN (left) and RMN + UAVs (middle and right). **Bottom row**: Using data from the UAVs only.

trajectories of the UAVs as well as the contours of the total cloudshine dose correspond very well with the results obtained using the RMN, Fig. 5.

Reliability of the estimation was tested via the figure of merit in space (FMS) measure (Abida and Bocquet, 2009),

$$\mathrm{FMS} = \frac{\sum_{\boldsymbol{s}\in S} \min\left(\widehat{D}(\boldsymbol{s}), D_{\mathrm{twin}}(\boldsymbol{s})\right)}{\sum_{\boldsymbol{s}\in S} \max\left(\widehat{D}(\boldsymbol{s}), D_{\mathrm{twin}}(\boldsymbol{s})\right)}, \tag{25}$$

where $\widehat{D}(\boldsymbol{s})$ denotes expected value of the total cloudshine dose at location $\boldsymbol{s}$, and $D_{\mathrm{twin}}(\boldsymbol{s})$ is the dose for the twin model. Box plots with this measure for 50 random simulations are displayed in Fig. 7. Note that the FMS of the assimilation without the UAVs is decreasing due to the incorrectly estimated wind bias, while all scenarios with the UAVs are able to correctly determine the wind direction bend and improve the FMS. The differences between the three considered loss functions are negligible since differences in informativeness of the measurements are small.

As expected, the scenarios using only the UAV measurements have lower FMS than those using the RMN. Interestingly, the loss of performance is usually lesser than 10%. The flexibility of the UAVs is able to compensate the lack of sensors in the RMN. This is a very promising result for applications where the RMN is not available.

4.4. Continuous release

The scenario in Section 4.1 is favorable for the UAVs since the radioactive cloud is relatively small, and its tracking is equivalent to flying with the cloud. Continuous release of the radioactive material is more demanding for assimilation since the uncertainty in the concentration is distributed over the whole plume due to the random walk model on the wind field biases given by Equations (7)–(9). A rapid change in the wind direction (which is assumed to have high probability) would shift the whole plume.

A continuous release was simulated with the same weather conditions as those in Section 4.1, but the release does not end after one hour, but keeps repeating the same release profile, see Fig. 8. As in the short release, the measurements from the RMN are informative about the released activity and the resulting estimates are accurate. Estimates obtained using only the measurements from the UAVs have significantly higher variance.

Typical values of the assimilated contour plot of the total cloudshine dose for all scenarios are displayed in Fig. 9, for scenarios using the RMN, RMN + UAVs, and UAVs only. Position of the UAVs in all time steps is also displayed where appropriate. In this case, the UAVs can not simply follow a cloud disconnected from the source but they have to monitor the full area of the plume. In the RMN + UAVs scenario, the UAVs move in the area of the RMN for the first few time steps. When the plume leaves the area covered by the RMN, the first UAV follows the plume and when it is sufficiently far away from the RMN, the second UAV also follows. However, in this case, the UAVs often goes forward and back, and in effect, patrol the area. In the UAVs only scenario, the UAVs patrol exactly the area covered by the first ring of the RMN, see Fig. 9 right (detail). Hence, they are not able to obtain informative measurements about the wind field biases in the distant parts of the monitored area.

Quantitative comparison of the assimilation results in terms of the FMS is displayed in Fig. 10. As expected, the best results are obtained in the RMN + UAVs scenario. The RMN and UAVs scenarios achieve very similar results, with the UAVs scenario being slightly worse. Note however, that the UAVs have only 2 radiation sensors compared to 32 sensors of the RMN. It is the flexibility in navigation of the UAVs that allows to compensate for the missing sensors. Note

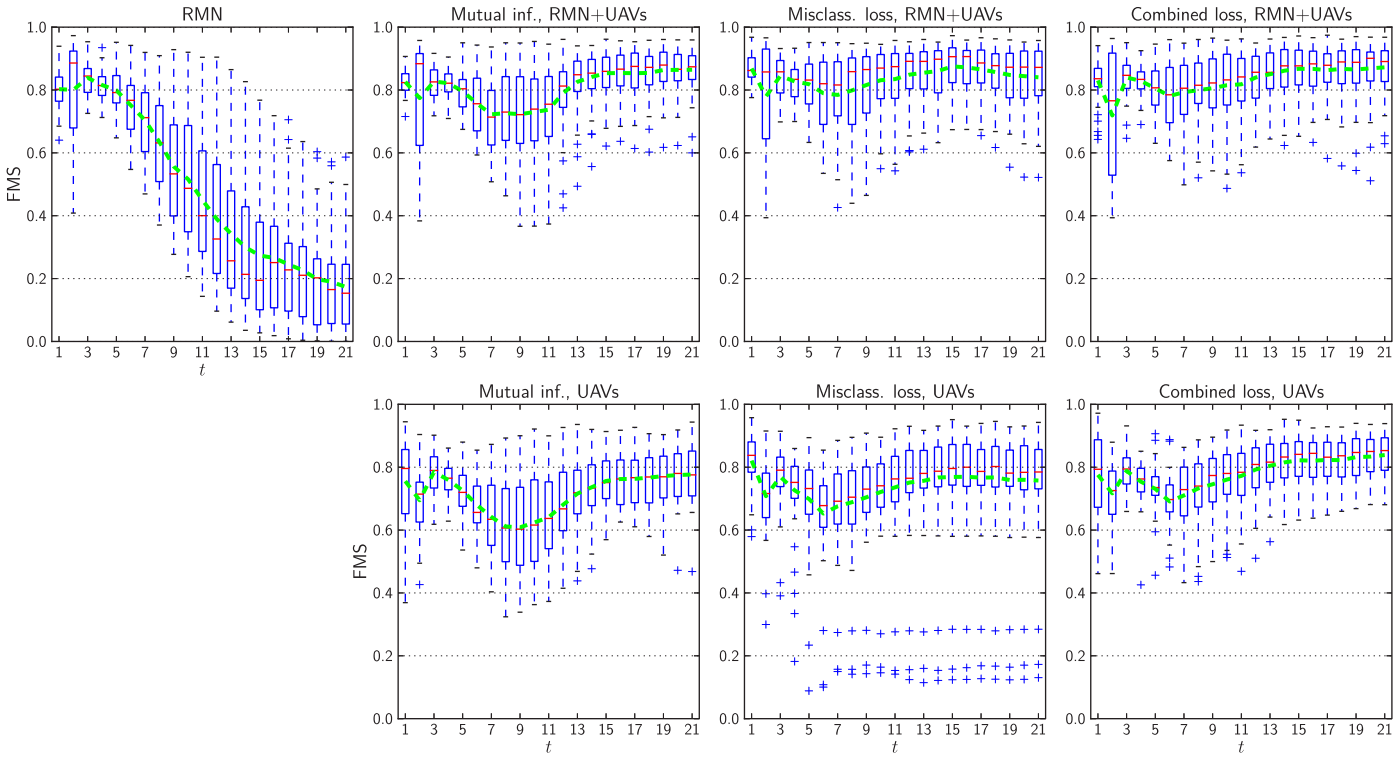

Fig. 7. Box-plots of FMS (25) for all considered assimilation scenarios.

however, that there were also few poor realizations in the box-plot of the FMS in the UAVs only scenario. In these cases, the realization of the random variables resulted in navigation of the UAVs to the positions with no measurable gamma dose from the plume and thus incorrect estimate of the released activity.

4.5. Potential extensions of the approach

The presented results were obtained using a simple dispersion model and a simple correction model of the numerical weather forecast. However, the same methodology can be applied to an arbitrary dispersion model and an arbitrary weather correction model since the underlying particle filter can handle any type of complex models with uncertainty. Extensions to different models are then straightforward. The necessary issue that needs to be resolved for more complex models is the computational feasibility of the particle filter. Due to the use of sophisticated proposal function (22) designed for the considered models, evaluation of the simulation with assimilation and UAVs navigation of the 3 h release for 99 particles took about 7 min on a i7 quadcore processor. However, computational requirements can dramatically increase for more unknown parameters, more demanding conditions, or unoptimized non adaptive proposal functions (such as the bootstrap filter).

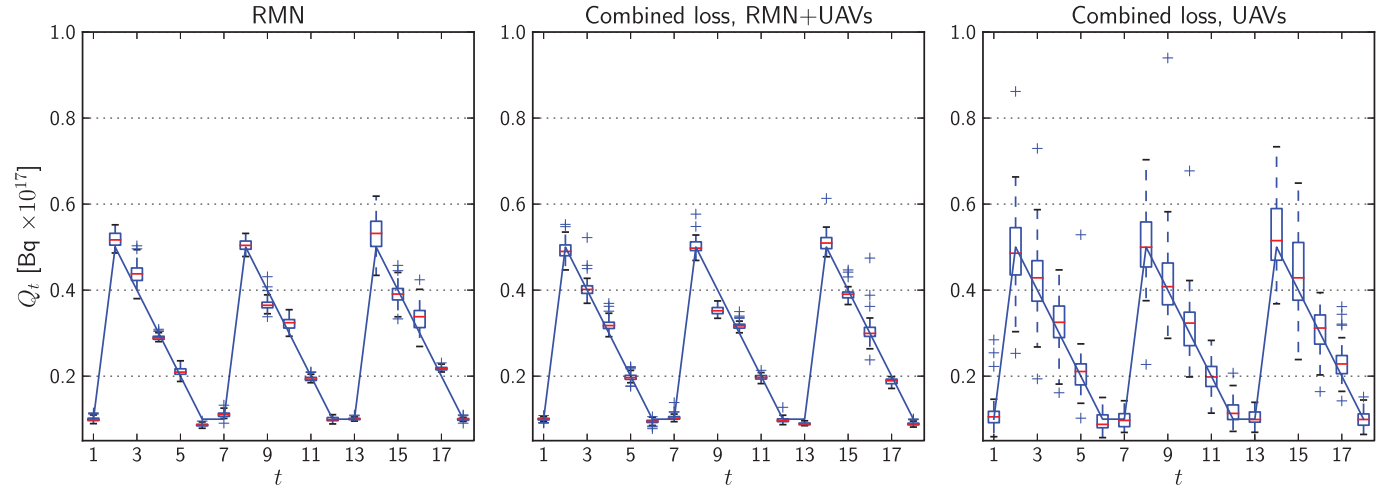

Fig. 8. Released activity in the continuous release and its estimates under different scenarios. Solid lines represent the values simulated in the twin model.

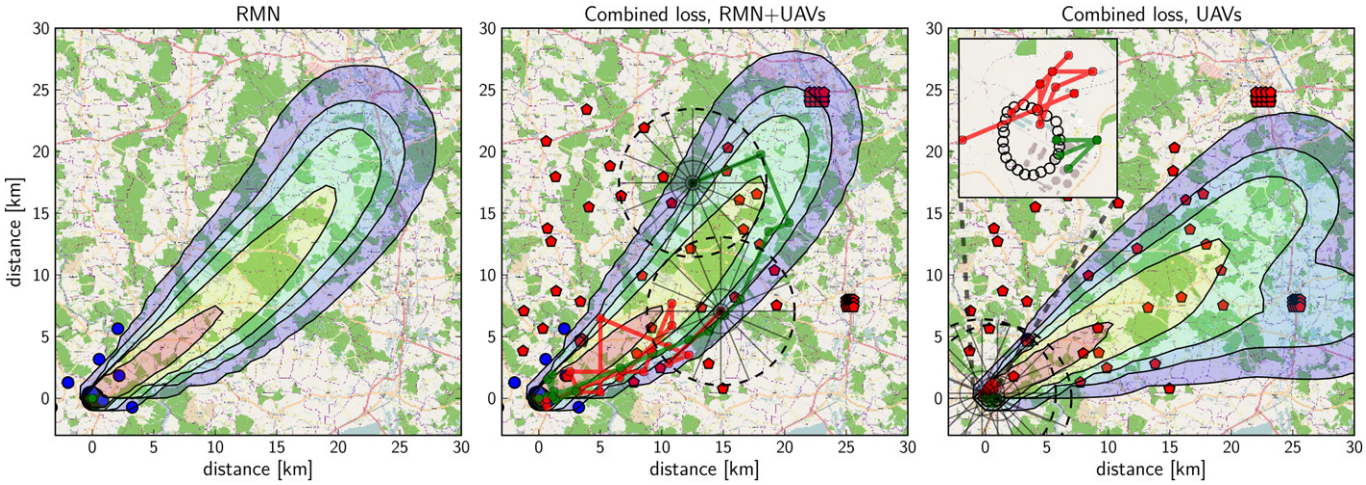

Fig. 9. Contour plots of the total cloudshine dose assimilated under different scenarios.

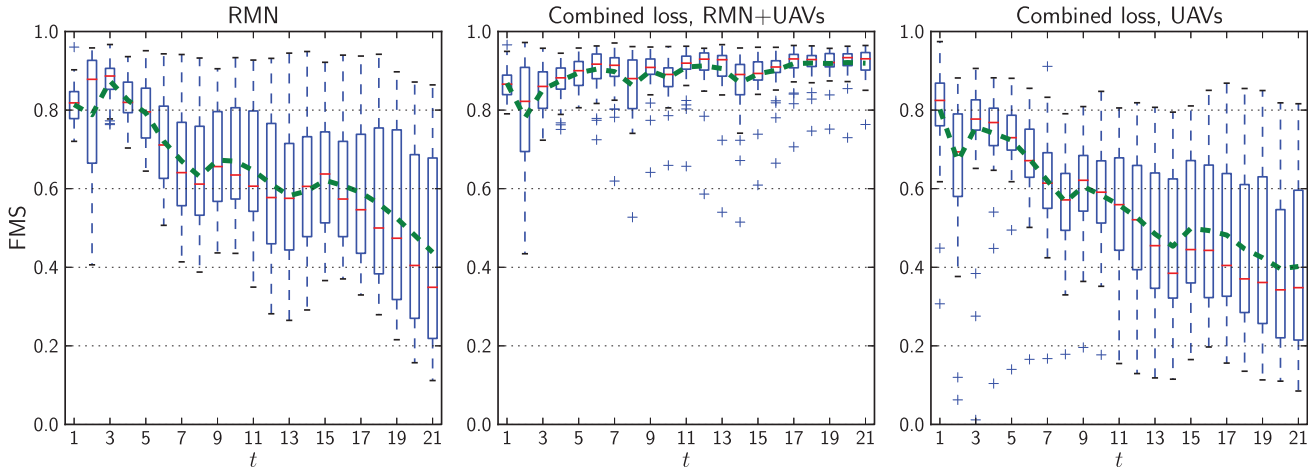

Fig. 10. Box plot of the FMS for different assimilation scenarios from 50 random simulations.

5. Conclusion

Monitoring of an atmospheric release is a demanding task due to uncertainty in the parameters of the release and variability of the weather conditions. Every measurement of the pollutant concentration or local meteostation improves the results of the data assimilation. Traditionally, the monitoring sensors were assumed to be stationary, with potential extension for mobile measuring stations. In this paper, we have extended the idea of mobile stations to the autonomously navigated unmanned aerial vehicles (UAVs). In a series of synthetic experiments we have shown that the UAVs suitably complement the existing monitoring networks especially in cases where the numerical weather forecast is biased from the reality. Due to the possibility of vertical movement, the UAVs can allow monitoring of parameters that the existing networks has difficulty with, such as the release height. Extending existing networks with UAVs can thus bring significant improvement in radiation safety monitoring systems.

Moreover, the flexibility of the UAVs allows their independent use as an adaptive monitoring network. We have shown that as few as two UAVs are able to provide assimilation results of quality comparable to that of the stationary monitoring network. In simple scenarios, such as a short release of a pollutant, the UAVs outperform the stationary network. On the other hand, the Monte Carlo study revealed increased variance of the assimilation results in the case of the UAV-only scenario. Reliable operation in this scenario would require to increase the optimization horizon and to compute more particles than is needed when UAVs are used as a complement of the stationary network. Further work is clearly needed to reach that goal.

Appendix A. Particle filter for data assimilation

Initialization: sample state variable $[Q_0, \boldsymbol{\theta}_0]$ from prior densities,
At each time t do:

1 Collect measurements $\boldsymbol{y}_t$
2 For each particle, do
(a) Update shaping parameters $\alpha_{v,t}, \beta_{v,t}$ using (A.1), and $\widehat{\theta}_{\phi c,t}, P_{\phi c,t}$ using (A.2).
(b) Sample new values of $\theta_{v,t}^{(n)}$ from $\mathcal{G}(\alpha_{v,t}, \beta_{v,t})$, and $\theta_{\phi c,t}^{(n)}$ from.
(c) Compute new locations of all puff centers $\boldsymbol{l}_t^{(n)}$ using (5), (6) and (10).
(d) Evaluate radiation dose coefficients $\rho_{k,j,t}$ for each receptor.
(e) Optimize shaping parameters $\widehat{Q}_t, \sigma_{Q,t}$ using Newton Raphson algorithm (Appendix B) and sample new values $Q_t^{(n)}$ from the resulting proposal density $\mathcal{N}(\widehat{Q}_t, \sigma_{Q,t}^2)$.
(f) Evaluate weights $w_t^{(i)}$ using (19) and normalize them.
3 Resample the particles.

Appendix A.1. Optimal proposal densities for the wind field correction

Since the prior on the wind speed was chosen to be Gamma density and the density of the observation is of the inverse Gamma type, the optimal proposal can be computed using conjugate update (Bernardo and Smith, 1997):

$$\begin{aligned} q(\theta_{v,t}|\boldsymbol{y}_t,\theta_{v,t-1}) &= \mathcal{G}(\alpha_{v,t},\beta_{v,t}) \ , \\ \alpha_{v,t} &= \frac{v_{t-1}^2}{\gamma_{\theta v}v_{t-1}^2+v_{\theta 0}}+\gamma_v^{-1}+1, \\ \beta_{v,t} &= \frac{v_{t-1}^2}{\gamma_{\theta v}v_{t-1}^2+v_{\theta 0}}(\theta_{v,t-1})^{-1}+\tilde{v}_t v_t^{-1}\left(\gamma_v^{-2}+1\right). \end{aligned} \tag{A.1}$$

Since the random walk model on $\theta_{\phi,t}$ and $\theta_{c,t}$ is Gaussian and the observations are also Gaussian, Equation (7) form a linear state $\theta_{\phi c,t}=[\theta_{\phi,t},\theta_{c,t}]$, with evolution model

$$\theta_{\phi c,t}=\theta_{\phi c,t-1}+Q^{-\frac{1}{2}}e_t, \quad Q=\begin{bmatrix}\gamma_\phi^2 & 0\\ 0 & \gamma_c^2\end{bmatrix},$$

and observation equations

$$\boldsymbol{y}_{\phi,t}=\begin{bmatrix}\phi_{\text{meteostation},t}\\ \phi_{\text{UAV1},t}\\ \phi_{\text{UAV2},t}\end{bmatrix}=C\begin{bmatrix}\theta_{\phi,t}\\ \theta_{c,t}\end{bmatrix}+R^{-\frac{1}{2}}\varepsilon_t,$$

$$C=\begin{bmatrix}1 & 0\\ 1 & \|\boldsymbol{s}_{\text{meteostation}}-\boldsymbol{s}_{\text{UAV1}}\|\\ 1 & \|\boldsymbol{s}_{\text{meteostation}}-\boldsymbol{s}_{\text{UAV2}}\|\end{bmatrix}, \quad R=\sigma_\phi^2 I_3,$$

where e_t and ϵ_t are Gaussian distributed errors, and I_3 denotes 3×3 identity matrix. The optimal proposal density is then given by the Kalman filter:

$$\begin{aligned} q\left(\theta_{\phi c,t}|\boldsymbol{y}_t,\theta_{\phi c,t-1}\right) &= \mathcal{N}\left(\widehat{\theta}_{\phi c,t},P\right), \\ \widehat{\theta}_{\phi c,t} &= \theta_{\phi c,t-1}+K\left(\boldsymbol{y}_{\phi,t}-C\theta_{\phi c,t-1}\right), \\ K &= QC^TR, \quad P=(I-KC)Q. \end{aligned} \tag{A.2}$$

Appendix A.2. Laplace approximation for proposal of the released dose

The task is to approximate the optimal proposal density which is a product of inverse Gamma likelihood (21) and Gamma prior (3). The Bayes rule yields

$$\begin{aligned} p(Q_t|\boldsymbol{y}_t) &\propto p(Q_t)p(\boldsymbol{y}_t|Q_t)\propto Q_t^{\alpha_Q-1}\exp(-Q_t\beta_Q) \\ &\times\prod_{j=1}^{m}(\kappa_{j,t}Q_t+m_{j,t})^{\alpha_y}y_{j,t}^{-\alpha_y-1}\exp\left(-\frac{\kappa_{j,t}Q_t+m_{j,t}}{y_{j,t}}\right), \end{aligned} \tag{A.3}$$

where (20) was rewritten using $\kappa_{j,t}=(\alpha_y-1)\rho_{t,j,t}$, and $m_{j,t}=\sum_{k=1}^{t-1}Q_k\rho_{k,j,t}+c_{bg}$. This density is not in a standard form and the normalization can not be obtained analytically. We propose to approximate (A.3) using Laplace approximation (Kass et al., 1990). Specifically, we approximate (A.3) by a probability density at its maximum value:

$$\widehat{Q}_t=\arg\max_{Q_t}(\log(p(Q_t|y_t))). \tag{A.4}$$

The first derivative of logarithm of (A.3) is:

$$\frac{\mathrm{dlog}(p(Q_t|y_t))}{\mathrm{d}Q_t}=\sum_{j=1}^{m}\left[\frac{\alpha_y\kappa_{j,t}}{\kappa_{j,t}Q_t+m_{j,t}}-\frac{\kappa_{j,t}}{y_{j,t}}\right]+\frac{\alpha_Q-1}{Q_t}-\beta_Q. \tag{A.5}$$

Function (A.4) has only one maximum that can be found using the Newton Raphson method. Once the maximum value is established, we compute the second derivative of (A.5) at point $\widehat{Q}_t$ and set it equal to inverse covariance matrix of the Normal density:

$$\frac{1}{2}\sigma_Q^{-2}=\sum_{j=1}^{m}\left[\frac{\alpha_y\kappa_{j,t}^2}{\left(\kappa_{j,t}\widehat{Q}_t+m_{j,t}\right)^2}\right]+\frac{\alpha_y-1}{\widehat{Q}_t^2},$$

to form the proposal density $q(Q_t|\boldsymbol{y}_t)=\mathcal{N}(\widehat{Q}_t,\sigma_Q^2)$.

References

Abida, R., Bocquet, M., 2009. Targeting of observations for accidental atmospheric release monitoring. Atmospheric Environment 43 (40), 6312–6327.

Abida, R., Bocquet, M., Vercauteren, N., Isnard, O., 2008. Design of a monitoring network over France in case of a radiological accidental release. Atmospheric Environment 42 (21), 5205–5219.

Berger, J., 1985. Statistical Decision Theory and Bayesian Analysis. Springer, New York.

Bernardo, J., Smith, A., 1997. Bayesian Theory, second ed. John Wiley & Sons, Chichester, New York, Brisbane, Toronto, Singapore.

Caselton, W., Husain, T., 1980. Hydrologic networks: information transmission. Journal of the Water Resources Planning and Management Division 106 (2), 503–520.

Cervone, G., Franzese, P., Grajdeanu, A., 2010. Characterization of atmospheric contaminant sources using adaptive evolutionary algorithms. Atmospheric Environment 44 (31), 3787–3796.

Doucet, A., de Freitas, N., Gordon, N. (Eds.), 2001. Sequential Monte Carlo Methods in Practice. Springer.

Gordon, N., Salmond, D., Smith, A., 1993. Novel Approach to Nonlinear/non-Gaussian Bayesian State Estimation, vol. 140. IEE, pp. 107–113.

Haupt, S., Beyer-Lout, A., Long, K., Young, G., 2009. Assimilating concentration observations for transport and dispersion modeling in a meandering wind field. Atmospheric Environment 43 (6), 1329–1338.

Heuvelink, G., Jiang, Z., De Bruin, S., Twenhöfel, C., 2010. Optimization of mobile radioactivity monitoring networks. International Journal of Geographical Information Science 24 (3), 365–382.

Hiemstra, P., Karssenberg, D., van Dijk, A., 2011. Assimilation of observations of radiation level into an atmospheric transport model: a case study with the particle filter and the ETEX tracer dataset. Atmospheric Environment, 6149–6157.

Hoffmann, G., Tomlin, C., 2010. Mobile sensor network control using mutual information methods and particle filters. IEEE Transactions on Automatic Control 55 (1), 32–47.

Jeong, H., Kim, E., Suh, K., Hwang, W., Han, M., Lee, H., 2005. Determination of the source rate released into the environment from a nuclear power plant. Radiation Protection Dosimetry 113 (3), 308.

Johannesson, G., Hanley, B., Nitao, J., 2004. Dynamic Bayesian Models Via Monte Carlo – an Introduction With Examples. Tech. Rep., Lawrence Livermore National Laboratory.

Kass, R., Tierney, L., Kadane, J., 1990. The validity of posterior expansions based on laplace's method. Bayesian and Likelihood Methods in Statistics and Econometrics 7, 473–488.

Kovalets, I., Tsiouri, V., Andronopoulos, S., Bartzis, J., 2009. Improvement of source and wind field input of atmospheric dispersion model by assimilation of concentration measurements: method and applications in idealized settings. Applied Mathematical Modelling 33 (8), 3511–3521.

Kuroki, Y., Young, G., Haupt, S., 2010. UAV navigation by an expert system for contaminant mapping with a genetic algorithm. Expert Systems with Applications 37 (6), 4687–4697.

Mardia, K., Jupp, P.E., 2000. Directional Statistics. John Wiley and Sons, Chichester, England.

Melles, S., Heuvelink, G., Twenhöfel, C., van Dijk, A., Hiemstra, P., Baume, O., Stöhlker, U., 2011. Optimizing the spatial pattern of networks for monitoring radioactive releases. Computers & Geosciences 37 (3), 280–288.

Pecha, P., Hofman, R., Šmídl, V., 2009. Bayesian tracking of the toxic plume spreading in the early stage of radiation accident. In: Proceeding of European Simul. and Modelling Conference ESM.

Skoglar, P., 2009. Planning Methods for Aerial Exploration and Ground Target Tracking. Tech. Rep. 1420, Linköping University.
Šmídl, V., Hofman, R., 2011. Bayesian methods for optimization of radiation monitoring networks. Tech. Rep. 2315, UTIA.
Šmídl, V., Hofman, R., 2012a. Application of sequential monte carlo estimation for early phase of radiation accident. Tech. Rep. 2322, UTIA.
Šmídl, V., Hofman, R., 2012b. Navigation of UAVs for tracking of atmospheric release of radiation. In: CDC 2012, IEEE Conference on Decision and Control. Accepted.
Thompson, I., Andersen, C., Bøtter-Jensen, L., Funck, E., Neumaier, S., Sáez-Vergara, J., 2000. An international intercomparison of national network systems used to provide early warning of a nuclear accident having transboundary implications. Radiation Protection Dosimetry 92 (1–3), 89.
Thykier-Nielsen, S., Deme, S., Mikkelsen, T., 1999. Description of the Atmospheric Dispersion Module RIMPUFF. Riso National Laboratory, PO Box 49.
van den Kroonenberg, A., Martin, T., Buschmann, M., Bange, J., Vörsmann, P., 2008. Measuring the wind vector using the autonomous mini aerial vehicle M2AV. Journal of Atmospheric and Oceanic Technology 25 (11), 1969–1982.
Zidek, J., Sun, W., Le, N., 2000. Designing and integrating composite networks for monitoring multivariate gaussian pollution fields. Journal of the Royal Statistical Society: Series C (Applied Statistics) 49 (1), 63–79.